

A Smooth Transition from Giant Planets to Brown Dwarfs from the Radial Occurrence Distribution

JUDAH VAN ZANDT,^{1,*} GREGORY J. GILBERT,^{1,2} ERIK A. PETIGURA,¹ STEVEN GIACALONE,^{2,†} ANDREW W. HOWARD,² AND LUKE B. HANDLEY²

¹*Department of Physics & Astronomy, University of California Los Angeles, Los Angeles, CA 90095, USA*

²*Department of Astronomy, California Institute of Technology, Pasadena, CA 91125, USA*

ABSTRACT

Measuring the occurrence rates of celestial objects is a valuable way to study their origins and evolution. Giant planets and brown dwarfs produce large Doppler signatures that are easily detectable by modern instrumentation, and legacy radial velocity (RV) surveys have now achieved full orbital coverage for periods $\lesssim 30$ years. However, the Doppler method’s sensitivity to companion minimum mass $M_c \sin i$ — as opposed to true mass M_c — prevents unambiguous characterization using RVs alone, as purported giant planets may be brown dwarfs or stars on inclined orbits. Here we combined legacy RVs with absolute astrometry to re-fit the orbits of 195 companions from the California Legacy Survey. Nearly 50% (8/18) of the “brown dwarfs” ($M_c \sin i = 13\text{--}80 M_{\text{Jup}}$) we refit had true masses above $80 M_{\text{Jup}}$. We incorporated our orbital posteriors and target sensitivity maps into a Poisson likelihood model to calculate occurrence as a function of true companion mass M_c ($0.8\text{--}80 M_{\text{Jup}}$) and separation a (0.3–30 AU). The semi-major axis distributions of objects in this range vary smoothly with mass, with Jupiter analogs favoring an abrupt increase in occurrence near 1 AU and brown dwarfs exhibiting a gradual enhancement at wider separations. Marginalized companion occurrence between 1–10 AU decreases smoothly with mass, with brown dwarfs having the lowest occurrence rate: $0.9_{-0.4}^{+0.5}\%$. Jupiter analogs are 10 times as common as brown dwarfs per mass interval in this range, demonstrating that the brown dwarf desert extends to 10 AU. The smooth variation in these distributions disfavors a sharp transition mass between “bottom-up” core accretion and “top-down” gravitational instability formation mechanisms, and rather suggests that these processes may produce companions in overlapping mass ranges.

1. INTRODUCTION

Understanding how giant planets and brown dwarfs form is a key question in exoplanet science. Planets below $1 M_{\text{Jup}}$ are thought to form “bottom-up” through the collision of small planetesimals and subsequent runaway accretion of a gaseous envelope (Pollack et al. 1996; Youdin & Zhu 2025). Meanwhile, objects above $80 M_{\text{Jup}}$ form “top-down” by direct gravitational collapse of molecular clouds, and have sufficiently large masses to sustain core hydrogen burning (McKee & Ostriker 2007; Shu et al. 1987). Intermediate-mass objects ($1\text{--}80 M_{\text{Jup}}$) may occupy a region of overlap between these processes, with some larger objects forming through core accretion and smaller ones through direct

collapse. Other formation channels could contribute in this regime as well, such as collapse due to gravitational instability of the protoplanetary disk (e.g. Kratter & Lodato 2016).

The distributions of intermediate-mass companion properties, such as their masses, orbital separations, and eccentricities, are useful tracers of their formation histories and may illuminate their relationship to the planetary and stellar populations. Companion occurrence near the ice line (1–10 AU) is particularly important due to the role that icy planetesimals play in planet formation (Drażkowska & Alibert 2017). At present, detecting companions at separations near 10 AU is difficult. Direct imaging efforts have measured the prevalence of giant planets ($M_c \sim 5\text{--}13 M_{\text{Jup}}$) and brown dwarfs ($M_c \sim 13\text{--}80 M_{\text{Jup}}$) out to hundreds of AU, using evolutionary models (e.g. Lagrange et al. 2025; Wilkinson et al. 2024; Baraffe et al. 2003) and recently, dynamical measurements incorporating absolute astrometry (e.g. Franson et al. 2023; Currie et al. 2023) to estimate these

Corresponding author: Judah Van Zandt
 judahvz@astro.ucla.edu

* NASA FINESST Fellow

† NSF Astronomy and Astrophysics Postdoctoral Fellow

objects' masses. With a few notable exceptions, such as 51 Eridani b (Macintosh et al. 2015), β Pictoris b (Bonnefoy et al. 2014), and AF Leporis b (Franson et al. 2023; Currie et al. 2023; De Rosa et al. 2023), imaging has historically been unable to probe separations closer than ~ 10 AU due to the high contrast between close companions and their host stars (see Bowler & Nielsen 2018 for a review). Meanwhile, few RV surveys have compiled the 30-year observing baselines needed to measure complete orbits of companions at 10 AU; these objects' signatures instead manifest as partial orbits which are difficult to distinguish from those caused by brown dwarfs and stellar companions.

One of the few RV samples that is sensitive out to 10 AU is the California Legacy Survey (CLS; Rosenthal et al. 2021). Using this sample's multi-decade RV data sets, Fulton et al. (2021) found that giant planet occurrence peaks between 1–10 AU and falls off at wider separations. The RV technique's sensitivity to companion minimum mass rather than true mass introduces ambiguity into the results of any Doppler survey. Given the high intrinsic prevalence of planetary objects (Petigura et al. 2018; Rosenthal et al. 2022), the probability of highly-inclined stars or brown dwarfs masquerading as planets is low. However, brown dwarfs are rare compared to stellar companions (Raghavan et al. 2010), resulting in a substantial probability that RV-discovered brown dwarfs are in fact inclined stars. Resolving the $M_c \sin i$ ambiguity is therefore crucial to accurately measuring the occurrence of substellar companions.

In this study, we re-fit the RVs of 128 systems in the CLS, incorporating astrometric data from the *Hipparcos-Gaia* Catalog of Accelerations (HGCA; Brandt 2021) when available, to constrain the inclinations and true masses of 195 stellar, substellar, and planetary companions (Sections 2 and 3). We present the occurrence of planets and brown dwarfs in this sample and note mass and semi-major-axis ranges with high and low formation efficiency (Section 4). Finally, we consider the implications of our measurements on formation of these objects (Section 5).

2. OBSERVATIONS

2.1. California Legacy Survey

The California Legacy Survey (CLS; Rosenthal et al. 2021) monitored the radial velocities (RVs) of 719 bright ($V \approx 6$ –10), nearby ($d \approx 8$ –60 pc) stars for more than 30 years. In total, this dataset includes 100,000 RVs from the Keck/HIRES, APF/Levy, and Lick/Hamilton spectrographs. In this sample, Rosenthal et al. (2021) identified 226 companions with the following distribution of minimum masses: 34 stars ($M_c \sin i > 80 M_{\text{Jup}}$),

19 RV brown dwarfs ($M_c \sin i = 13$ –80 M_{Jup}), and 173 RV planets¹ ($M_c \sin i < 13 M_{\text{Jup}}$). These detections spanned star-companion separations out to 20 AU and masses M_c down to $\sim 0.01 M_{\text{Jup}}$. The well-defined selection function of the CLS, as well as the uniform orbital analysis performed by Rosenthal et al. (2021), have made it a valuable resource for probing exoplanet demographics, particularly for planets at or near the water ice line (e.g. Fulton et al. 2021; Van Zandt & Petigura 2024a).

CLS measured their system-by-system sensitivity to companions through injection/recovery tests. In brief, an injection/recovery test consists of randomly drawing a set of orbital parameters (P, t_p, e, ω, K), modeling the RV signature that a companion with those parameters would produce, injecting that signature into a system's actual RV time series to capture system-specific RV noise and sampling inhomogeneities, and attempting to recover the signal with a planetary detection pipeline. CLS repeated this procedure 1000 times for each system, and estimated sensitivity as the fraction of successful recoveries in a given region of M_c - a space. We calculated CLS's survey-averaged sensitivity by combining the injection/recovery tests of all stars in the sample. We show this average map, together with the CLS catalog, in both panels of Figure 1.

2.2. *Hipparcos-Gaia* Catalog of Accelerations

The *Hipparcos-Gaia* Catalog of Accelerations (HGCA; Brandt 2021) provides astrometric proper motion measurements for over 115,000 stars calculated by aligning the *Hipparcos* reference frame (Hip 1997) with that of *Gaia* EDR3 (Lindegren et al. 2021). The HGCA lists three separate measurements of stellar proper motion: the *Hipparcos* and *Gaia* epoch proper motions, measured at approximately 1991.25 and 2016.0, respectively, as well as an average proper motion computed from the difference in the stellar position at these two epochs. By identifying changes in proper motion over time, one may infer the presence of massive long-period companions. The HGCA has found particular success in concert with other detection techniques, either by highlighting promising systems for follow-up observation (e.g., Franson et al. 2023) or by improving measurement precision through joint fitting (e.g., Van Zandt & Petigura 2024b; Zhang et al. 2025). Here we use the second approach, combining HGCA accelerations with

¹ Throughout this article, we use the terms “RV planet” and “RV brown dwarf” to refer to objects with minimum masses $< 13 M_{\text{Jup}}$ and 13 – $80 M_{\text{Jup}}$, respectively.

the multi-decade RV baselines of the CLS to fit orbits in three dimensions.

3. ANALYSIS

3.1. Joint RV/astrometry orbital fits

We refit the orbits of all 192 companions in the CLS with $M_c \sin i < 80 M_{\text{Jup}}$, plus three objects with $M_c \sin i > 80 M_{\text{Jup}}$ in systems with substellar companions, for a total of 195 orbital fits among 128 unique systems. We used `Orvara` (Brandt et al. 2021b) to fit three-dimensional orbits, parameterized by primary mass M_{pri} , companion mass M_c , semi-major axis a , eccentricity e , inclination i , argument of periastron of the companion orbit ω , longitude of ascending node Ω , parallax ϖ , and mean longitude at a reference epoch λ_{ref} . Fitting three-dimensional orbits allowed us to constrain companion true mass rather than $M_c \sin i$. `Orvara` supports joint fits of RV time series and absolute astrometry from both *Hipparcos* and *Gaia*, including modeling of the *Hipparcos* intermediate astrometric data and *Gaia* scanning law, through its integration of the `htof` astrometric fitting package (Brandt et al. 2021a).

We used the RV measurements provided in Rosenthal et al. (2021) for all systems. We incorporated astrometric accelerations from the HGCA for the 53 systems in which the acceleration was significant ($\frac{\Delta\mu}{\sigma_{\Delta\mu}} \geq 3$). In the remaining 75 systems, we supplied no astrometric data and fit only the RVs, allowing `Orvara` to marginalize over our uncertainty in inclination. The companions in systems with significant astrometric accelerations are indicated in the left panel of Figure 1. As expected, accelerating systems tend to host more massive companions: all but four systems exhibiting significant astrometric acceleration host at least one companion with $M_c > 1 M_{\text{Jup}}$.

We conducted orbital fits in stages, successively tuning our models for systems for which our MCMC simulations did not converge. For each system, we began with a model informed by the results of R21. We assumed the same number of companions they found, and bounded the range of companion eccentricity and semi-major axis at $\pm 4\sigma$ of their fitted values. In systems with significant trends, we included an additional companion to the model with a minimum separation of 10 AU. We widened the prior limits on eccentricity and/or semi-major axis for companions whose orbital posteriors were non-zero at the bounds. We applied `Orvara`'s default priors, including log-uniform priors on mass and semi-major axis. We applied this bounding procedure based on R21 in conjunction with standard priors merely to prevent the sampler from wandering into very low probability regions of parameter space where MCMC chains

were liable to become stuck; our use of R21 posteriors to inform the model initialization thus does not double-condition the data by introducing an erroneous prior.

We deviated from the above prescription for a handful of systems that required custom treatment. CLS reported two companions to **HD 167215**, one stellar and one substellar, at 7.2 and 8 AU, respectively. We found that the longer-period signal was likely a residual caused by an imperfect fit to the inner stellar companion orbit, and included only the latter in our model. CLS also reported an activity-induced false positive signal in the **HD 192310** system. We quoted their one-companion model parameters directly and marginalized over the companion's unknown inclination by dividing each $M_c \sin i$ sample by $\sin i$, with i drawn from a $\cos i$ -uniform distribution. We did the same for **HD 219134**, for which CLS reported five planets and three false positive signals associated with annual or instrumental systematics. For **HD 28185** we quoted the parameters fit by Venner et al. (2024), who incorporated 39 extra RVs into their analysis. Finally, we quoted CLS's orbital parameters and an inclination of 59° (Rivera et al. 2010) for the resonant system **GL 876**. Rivera et al. (2010) reported four planets in this system, but CLS found only three after ruling out multiple spurious signals. In a further eight systems, we included an additional long-period companion to model non-periodic RV variability. Given the large uncertainties on the fitted parameters of these companions, we did not include them in our occurrence calculations.

After removing the spurious substellar companion to HD 167215, we were left with 18 RV brown dwarfs ($M_c \sin i = 13\text{--}80 M_{\text{Jup}}$). Of these, eight had fitted true masses greater than $80 M_{\text{Jup}}$. We compare the original CLS catalog with our refit parameters in the left panel of Figure 1, and show the refit posteriors in the right panel.

3.2. Occurrence Framework

We modeled planet occurrence as a piecewise constant function, that is, a histogram, in companion mass M_c and semi-major axis a . We assumed that the companion occurrence rate in each histogram bin was independent of those in other bins.

Following previous studies (e.g., Foreman-Mackey et al. 2014; Fulton et al. 2021; Van Zandt et al. 2025), we modeled our catalog as a series of draws from a censored Poisson point process defined by the companion occurrence rate density (ORD) $\lambda(\log a, \log M_c | \boldsymbol{\theta})$, which gives the number of companions per star per logarithmic a - M_c interval. We use $\boldsymbol{\theta}$ to denote the vector of model

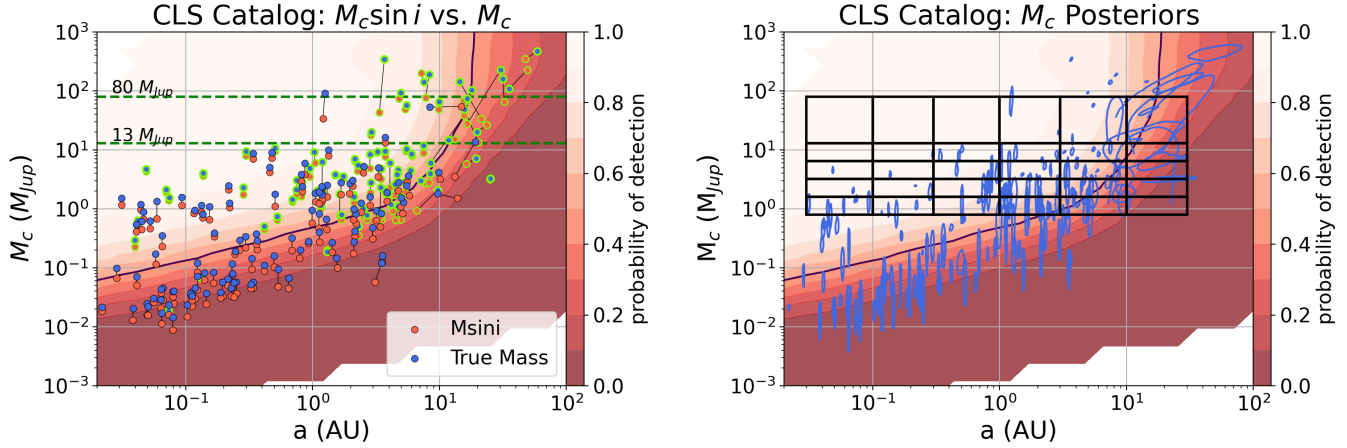


Figure 1. Left: The masses and semi-major axes of the substellar ($M_c \sin i \leq 80 M_{\text{Jup}}$) companions reported in the CLS catalog. Orange points show the average a and $M_c \sin i$ fitted, or in some cases quoted, by CLS, while blue points show the average a and M_c refitted in this work. Green borders indicate companions in whose orbital fits we included HGCA astrometry. The color map shows the CLS sensitivity to true mass, averaged over all 719 stars in the survey, with contours indicating sensitivity deciles and the 50% completeness line marked in black. Horizontal green lines mark 13 and $80 M_{\text{Jup}}$, the traditional brown dwarf mass limits. **Right:** Our re-fit catalog of 195 CLS companions. Contours enclose 68% of an individual companion’s posterior draws. Black rectangles indicate the cells in which we calculated companion occurrence (see Section 4). The completeness map is the same as in the right panel. Note that because the colored markers in the left panel indicate averages, companions with $M_c > 80 M_{\text{Jup}}$ may still have significant posterior mass below this limit, and vice versa.

parameters of λ , which for a histogram model is simply the bin heights.

Our full likelihood is given by

$$\mathcal{L} \propto e^{-\Lambda} \prod_{n=1}^{N_c} \lambda(\omega_n | \boldsymbol{\theta}) Q(\omega_n), \quad (1)$$

where we define $\omega = (\log a, \log M_c)$ for notational compactness. This likelihood function comprises two terms. The first gives the probability of N_c companion detections over the two-dimensional parameter space:

$$P(N_c | \boldsymbol{\theta}) = \frac{e^{-\Lambda} \Lambda^{N_c}}{N_c!}. \quad (2)$$

The Poisson rate parameter Λ gives the expected total number of observed companions among N_* host stars in the interval of interest:

$$\Lambda = N_* \int \lambda(\omega | \boldsymbol{\theta}) Q(\omega) d\omega, \quad (3)$$

where Q , the average sensitivity of the CLS to companions as a function of separation and true mass, accounts for missed companions.

The second term gives the probability that the N_c detected companions possess the set of observed parameters $\{\omega\}$:

$$P(\{\omega\} | N_c, \boldsymbol{\theta}) = \prod_{n=1}^{N_c} \frac{\lambda(\omega_n | \boldsymbol{\theta}) Q(\omega_n)}{\Lambda}. \quad (4)$$

We employed Equation 1 for each bin individually, treating the interval defined by the bin as the parameter space of interest and $\boldsymbol{\theta}$ as a single number giving the ORD in that bin.

Equation 1 gives the model likelihood in the case of negligible a and M_c uncertainties. We accounted for our non-negligible uncertainties as follows. We drew one sample from each companion posterior in our catalog to obtain a “catalog draw,” for which we then inferred a distribution of ORD values by evaluating Equation 1 over a fine grid in λ . We repeated this procedure 1000 times and averaged the resulting distributions to marginalize over our uncertainty in the true companion parameters. Our catalog sampling method ensured that detected companions influenced the inferred occurrence rate in a given bin in proportion to the fraction of their posterior mass that overlapped that bin.

4. RESULTS

4.1. Companion occurrence as a function of mass and semi-major axis

We measured occurrence as a function of both mass and separation in 30 cells defined by the following boundaries: $\frac{M_c}{M_{\text{Jup}}} = \{0.8, 1.6, 3.2, 6.4, 13, 80\}$, $\frac{a}{\text{AU}} = \{0.03, 0.1, 0.3, 1, 3, 10, 30\}$. We highlight our region of interest in the context of the CLS true mass catalog in the right panel of Figure 1. Figure 2 shows the results of these calculations. The drawback of calculating occurrence in 30 separate bin is that each bin

contains few companion detections, yielding large uncertainties on our measurements. We therefore performed a simple model comparison for the semi-major axis distribution of each mass bin: a step function versus a log-linear model, given respectively by

$$\lambda_a(a|a_0, C_1, C_2) = \begin{cases} C_1 & \text{if } a \leq a_0, \\ C_2 & \text{otherwise} \end{cases} \quad (5)$$

and

$$\lambda_a(a|m, b) = m \cdot \ln(a) + b, \quad (6)$$

where λ_a is a one-dimensional ORD, that is, the number of planets per star per semi-major axis interval.

We quantified the performance of each model by calculating the difference in Akaike Information Criterion (ΔAIC ; Akaike 1974) and Bayesian Information Criterion (ΔBIC ; Schwarz 1978) between the best-fit model and a constant (i.e., flat line) model. In all except the lowest-mass bin, we found a marginal preference for the log-linear model over the step function, indicating a gradual increase in occurrence at wider separations. In the lowest-mass bin, the preference for a step function suggests a more abrupt jump in occurrence near 1 AU. This preference, though modest in significance, is consistent with the expectation that the formation of Jovian planets through pebble accretion would benefit from the increase in planetesimals near the ice line (Drażkowska & Alibert 2017; Hyodo et al. 2019).

4.2. The Brown Dwarf Desert at 1–10 AU

One of the primary strengths of the CLS is its sensitivity to intermediate-separation companions ($\lesssim 10$ AU), uniting the outer limit of separations reached by RV surveys to the inner limit of those probed by direct imaging surveys (Bowler & Nielsen 2018). We measured the occurrence of giant companions ($0.8 < \frac{M_c}{M_{\text{Jup}}} < 80$) as a function of mass only, marginalizing over the separation interval 1–10 AU and using the same mass bins as in Section 4.1, with the exception of the brown dwarf bin (13 – $80 M_{\text{Jup}}$), which we divided at $32 M_{\text{Jup}}$. We found that the occurrence rate decreases monotonically with increasing mass, and that this trend persists in the occurrence rate density, which normalizes the occurrence rate in each mass interval by the interval size. We show the occurrence rate density distribution in Figure 3. The occurrence reaches a minimum for companions between 13 – $80 M_{\text{Jup}}$, demonstrating that the brown dwarf desert (Grether & Lineweaver 2006) extends to at least 10 AU.

4.3. A Rise in Giant Companion Occurrence at the Ice Line

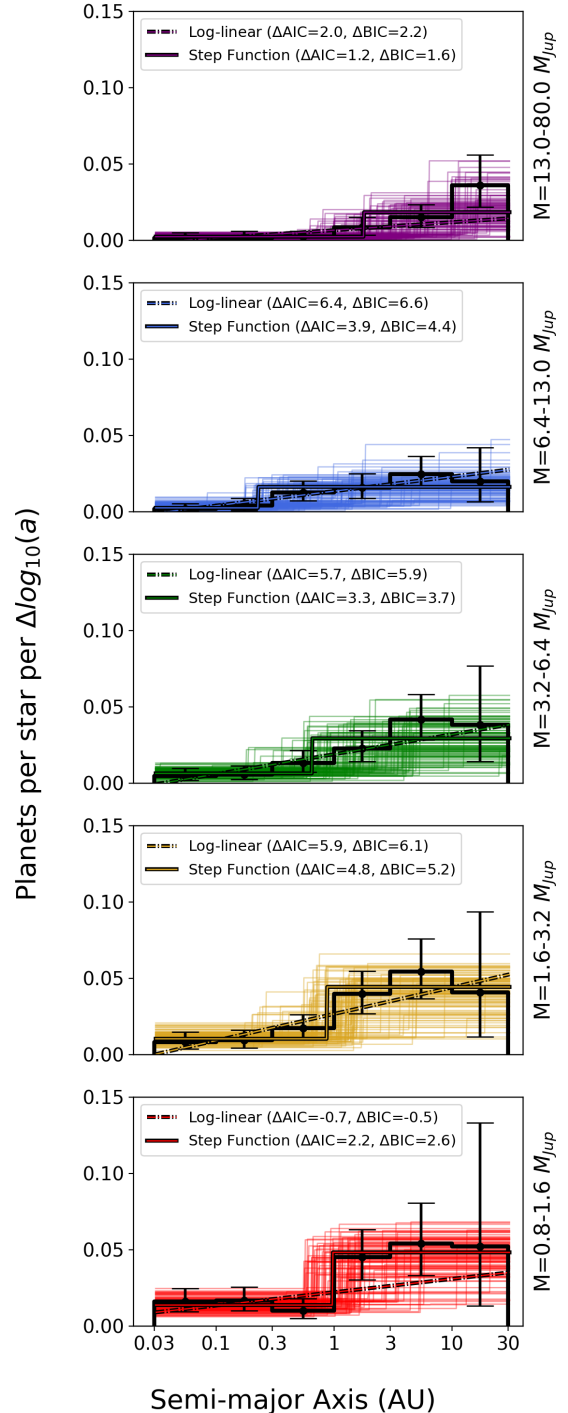


Figure 2. Radial occurrence rate density distributions for companions between 0.8 – $80 M_{\text{Jup}}$, with the highest-mass interval shown in the top panel. We fit each distribution with a log-linear model and a two-level step function. We calculated ΔAIC and ΔBIC values for the best-fit parameters for each model, using a constant model for comparison. In all cases we found that neither model was strongly preferred, though the step function was marginally preferred for companions with $M_c=0.8$ – $1.6 M_{\text{Jup}}$, a possible indication that the abundance of planetesimals near the ice line more strongly influences planet formation in this mass interval.

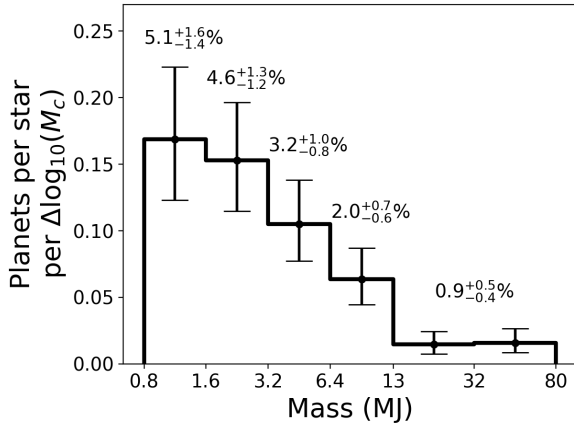


Figure 3. Marginalized occurrence rate density of CLS companions between 1–10 AU. Companion occurrence decreases log-linearly with increasing mass up to $\sim 20 M_{\text{Jup}}$, disfavoring a ‘cut-off’ mass at which companion formation near the ice line abruptly becomes inefficient. We annotate each mass bin with the true occurrence rate, quoting a single value for the range 13 – $80 M_{\text{Jup}}$ to facilitate comparison with other studies.

Finally, we examined the occurrence distribution of giant companions as a function of semi-major axis. We used the same separation bins as in Section 4.1, this time marginalizing over companion masses between 0.8 – $80 M_{\text{Jup}}$. We found that companion occurrence is approximately constant at close separations, increases abruptly near 1 AU, and remains enhanced to around 10 AU. There is also a marginally significant decrease in occurrence beyond 10 AU, though the uncertainty on our occurrence measurement between 10–30 AU prevents a firm conclusion. Figure 4 shows our marginalized semi-major axis distribution. Comparing this distribution with those we calculated for separate mass intervals (see Section 4.1), we see that the relatively high occurrence between 1–10 AU exhibited in the low-mass bins contributes to the rise at 1 AU in the marginalized distribution. Meanwhile, the small number of detections between 10–30 AU in any mass interval results in comparatively low occurrence in this range. We fit this distribution with both a two-level step function and a broken power law. We found that both models performed comparably well, and that the step location reliably fell near 1 AU.

We repeated these calculations using companion minimum mass and modified parameter bounds to match the analysis of Fulton et al. (2021), who calculated the semi-major axis distribution between 0.1–30 AU for companions with $M_c \sin i = 30$ – $6000 M_{\oplus}$ (0.09 – $18.9 M_{\text{Jup}}$). The maximum likelihood parameters of our broken power law fit to this occurrence distribution agreed closely with

those derived by Fulton et al. (2021), and we recovered the two key features noted in that study: an abrupt rise in occurrence near 1 AU and a possible fall-off beyond 10 AU. We obtained similar results after repeating our calculation for true mass instead of $M_c \sin i$. The persistence of the increase in occurrence near 1 AU — albeit at marginal significance — through changes in binning, mass limits, and M_c versus $M_c \sin i$ suggests that it is a robust feature of the radial occurrence distribution.

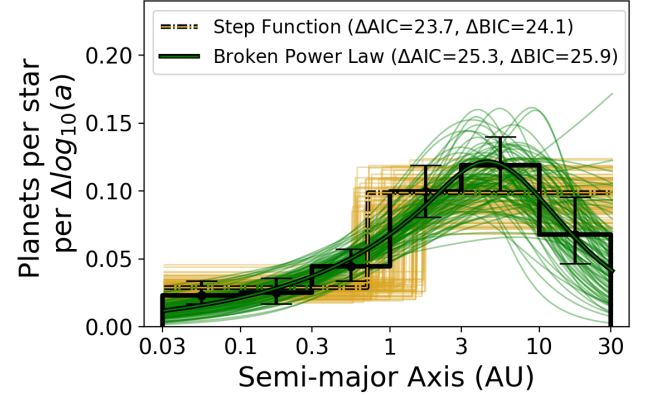


Figure 4. Occurrence rate density between 0.03 – 30 AU for companions between 0.8 – $80 M_{\text{Jup}}$. Companion occurrence is enhanced beyond 1 AU, and consistent with a decrease beyond 10 AU. A broken power law (solid green) and two-level step function (dotted yellow) fit the distributions comparably well, as measured by their ΔAIC and ΔBIC statistics compared to a constant occurrence rate model. Faded lines show posterior draws for each model. Nearly all steps occur between 0.5 and 1.7 AU.

5. DISCUSSION

5.1. An Astrophysically Motivated Planet-Brown Dwarf Divide

The International Astronomical Union defined brown dwarfs in 2003 as “substellar objects with true masses above the limiting mass for thermonuclear fusion of deuterium [$\sim 13 M_{\text{Jup}}$] ... no matter how they formed nor where they are located.”² This categorization had already been questioned by that time (Burrows et al. 2001), and has faced further scrutiny in the years since (e.g., Spiegel et al. 2011). Despite the benefit of providing an objective dividing line based on the measurable quantity M_c , there is no evidence that the processes that form giant planets and brown dwarfs are directly tied to the deuterium burning limit. To better address

² <https://web.archive.org/web/20141216075559/http://home.dtm.ciw.edu/users/boss/definition.html>

the nuances of companion formation at the planet-brown dwarf transition, astronomers have searched for definitions motivated by factors such as formation pathway, dynamics, and host star properties. [Schlaufman \(2018\)](#) found evidence for a divide between objects above/below $4\text{--}10 M_{\text{Jup}}$ based on the preference for objects below this range to orbit metal-rich host stars, a trait not exhibited by objects above it. Combining high-contrast imaging and astrometric observations between 5–100 AU, [Bowler et al. \(2020\)](#) found that companions with $M_c < 15 M_{\text{Jup}}$ have preferentially low eccentricities, peaking at $e \lesssim 0.2$, whereas higher-mass companions exhibit a broad range of eccentricities between $e=0.6\text{--}0.9$. Using a subset of the companion sample of [Bowler et al. \(2020\)](#) but a different framework for calculating parameter priors, [Do Ó et al. \(2023\)](#) found insufficient evidence for a distinction in the eccentricity distributions between low- and high-mass companions. Recent work by our team (Giacalone et al., in press; Gilbert et al., in press) examines the role of both metallicity and eccentricity in the planet-BD distinction in future work.

We searched for a similar distinction in the radial occurrence distributions of planets and BDs in Section 4.1. Among the five mass bins we analyzed, we did not find any abrupt change in the radial distributions with increasing mass. The lack of a sharp dividing line in mass among these distributions suggests that “bottom-up” and “top-down” formation mechanisms may produce companions in overlapping mass ranges. Because the majority of our cells contained fewer than five objects in this experiment, we were unable to constrain occurrence at high significance. Thus, some latent separation-dependent trends may exist that will provide a clearer dividing line between planets and brown dwarfs. On the other hand, we also found smooth variation with increasing mass for the marginalized occurrence distribution in Section 4.2, supporting the idea of a “fuzzy” planet-BD boundary.

We found marginal evidence for jumps in occurrence near 1 AU for companions between $0.8\text{--}3.2 M_{\text{Jup}}$. These features likely drive the analogous and more significant jump in the marginalized radial distribution (Section 4.3). Increased core accretion efficiency is expected near the ice line due to the enhancement of icy pebbles and silicate dust that can coagulate via gravitational and/or streaming instabilities in this region ([Drażkowska & Alibert 2017; Hyodo et al. 2019](#)). Thus, the presence or absence of an abrupt increase in occurrence near the ice line may be used to infer whether an object formed by core accretion or gas/disk instability. Increased Doppler baselines, larger stellar samples, and superior orbital fits through the inclusion of Gaia DR4

astrometry ([Winn 2022](#)) will enable occurrence measurements precise enough to confirm or rule out an occurrence jump in narrow mass intervals such as those examined here. Such measurements will place an astrophysically motivated planet-brown dwarf dividing line within reach.

5.2. The Brown Dwarf Desert

We showed in Section 4.2 that occurrence decreases with increasing mass, reaching a minimum for brown dwarfs ($13\text{--}80 M_{\text{Jup}}$). This interval extends to a mass ratio ($q = M_c/M_{\text{pri}}$) of approximately $q = 0.1$ for the Sun-like stars that comprise most of the CLS. Although we were unable to measure occurrence rates for higher-mass (stellar) companions, studies of stellar multiplicity over wide ranges in separation and primary type have found that the occurrence rate increases with increasing mass ratio for low q ($\sim 0.1\text{--}0.3$; [Reggiani & Meyer 2013; Moe & Di Stefano 2017](#)). Assuming this pattern holds for solar hosts between 1–10 AU, the $13\text{--}80 M_{\text{Jup}}$ interval represents a valley in the companion occurrence distribution, meaning that the brown dwarf desert found by [Grether & Lineweaver \(2006\)](#) for separations $\lesssim 3$ AU reaches, and perhaps exceeds, 10 AU.

The extension of the brown dwarf desert to at least 10 AU has ramifications for theories of brown dwarf dynamical evolution. In addition to a brown dwarf desert out to 5-year orbital periods (~ 3 AU), [Grether & Lineweaver \(2006\)](#) reported a lack of such a desert among free-floating BDs in the Orion, Pleiades, and M35 stellar clusters. In other words, brown dwarfs often form in isolation, but rarely as companions to Sun-like stars. They argued that this distinction disfavors a minimum in the efficiency of gravitational collapse or disk fragmentation ([Ida & Lin 2004](#)) as the source of the BD desert, and instead supports post-formation migration as the mechanism preventing the settlement of BDs at close separations. Our findings are consistent with this picture, but require that such migrations mechanisms be capable of explaining the BD desert out to 10 AU.

5.3. Comparison to Direct Imaging Surveys

The CLS’s achievement of sensitivity to companions near 10 AU is an important bridge between the short- and long-period regimes so far probed by RV and imaging surveys, respectively. It has allowed for comparison between occurrence rates calculated by these two methods ([Fulton et al. 2021](#)), under the assumption that giant planet occurrence remains constant between young (~ 10 Myr) and intermediate (Gyr) stellar ages.

In this work, we addressed a remaining barrier to direct comparison, which is the discrepancy between

the minimum masses measured by RVs alone and the true masses estimated from direct imaging through companion formation and luminosity models (Baraffe et al. 2003; Nielsen et al. 2019). We measured the occurrence of companions between 0.03–30 AU and 0.8–80 M_{Jup} , both as functions of mass and separation together (Section 4.1) and of each parameter separately (Sections 4.2 and 4.3).

In Section 4.2, we found an occurrence rate of $0.9^{+0.5\%}_{-0.4\%}$ for brown dwarfs ($M_c=13\text{--}80 M_{\text{Jup}}$) between 1–10 AU. Assuming the occurrence rate is log-constant at wide separations, this value is in close agreement with that of Nielsen et al. (2019), who estimated a BD occurrence rate of $0.8^{+0.8\%}_{-0.5\%}$ between 10–100 AU from observations made with the Gemini Planet Imager (Macintosh et al. 2014). If we extrapolate our BD occurrence rate between 10–30 AU ($1.7^{+1.0\%}_{-0.7\%}$) to 10–100 AU, assuming a log-uniform rate, we arrive at $3.4^{+2.0\%}_{-1.4\%}$, larger than the estimate of Nielsen et al. (2019). We note a number of caveats in our comparison: the large fractional uncertainties in both measurements, the difference in primary star masses and ages in the two samples, and the uncertainty in the period distribution of brown dwarfs between 10–100 AU.

5.4. Biases

Our study is subject to multiple biases, which we list here. First, we incorporated HGCA data into our fits only for systems exhibiting significant astrometric accelerations. Because larger companions produce more significant accelerations, our strategy allowed us to identify massive inclined companions, but was unable to precisely constrain the inclinations of their low-mass counterparts. This is analogous to the RV bias against low-mass, wide-separation objects, which we accounted for using a system-by-system sensitivity correction. A detailed accounting of the HGCA’s sensitivity would improve our result by accounting for the small inclined objects that the HGCA missed.

Another limitation in our analysis is the exclusion of RV trends. Long-period companions produce non-periodic signals that are consistent with a wide range of companion models, often including planets, brown dwarfs, and stars. Rosenthal et al. (2021) reported trends in 89 systems, nearly as many as the number of systems hosting companions with full orbits. Although it is possible to model such signals probabilistically (e.g. Van Zandt & Petigura 2024b; Van Zandt et al. 2025), we opted not to include them in our analysis due to their comparatively minor contribution to occurrence statistics in our parameter space of interest. A future study

incorporating trends would strengthen occurrence constraints, particularly at wide separations.

6. CONCLUSION

We re-fit the orbits of 192 substellar and 3 stellar companions from the California Legacy Survey to measure occurrence at wide separations ($\lesssim 30$ AU). We combined the multi-decade RV data sets of the California Legacy Survey with absolute astrometry from the *Hipparcos-Gaia* Catalog of Accelerations to fit three-dimensional orbits where possible. We identified eight of the 18 apparentlysubstellar companions ($M_c \sin i = 13\text{--}80 M_{\text{Jup}}$) in the CLS catalog as inclined M dwarfs.

We modeled companion occurrence as a Poisson point process in independent rectangular cells in $\log M - \log a$ space, accounting for survey sensitivity and uncertainties on fitted orbital parameters. We examined planet and BD occurrence as a function of both mass and separation. Our main conclusions are as follows:

- Nearly 50% of the RV brown dwarfs we refit were in fact low-mass stars, illustrating that populations of intrinsically rare objects are particularly susceptible to contamination from higher-mass companions on inclined orbits.
- The lack of a sharp transition between either the shape of the semi-major axis distributions of objects between 0.8–80 M_{Jup} (Section 4.1), or the marginalized occurrence rate between 1–10 AU (Section 4.2), disfavors a “cut-off mass” below which planets are exclusively formed by core accretion and above which brown dwarfs are exclusively formed by gravitational instability. Instead, the smooth variation in both distributions suggests that the two mechanisms produce companions in overlapping mass ranges.
- Companion occurrence between 1–10 AU is a monotonically decreasing function of mass, reaching a minimum for brown dwarfs ($13\text{--}80 M_{\text{Jup}}$), consistent with previous findings of a ‘brown dwarf desert’ at shorter separations. Whatever mechanism(s) stifle the formation/migration of brown dwarfs at low separations are relevant at wider separations as well.
- The radial occurrence distribution of all companions between 0.8–80 M_{Jup} exhibits a significant preference for a step near 1 AU, consistent with Fulton et al. (2021)’s finding of an enhancement in the occurrence of companions with $M \sin i = 30\text{--}6000 M_{\oplus}$ beyond 1 AU. Determining precisely which mass sub-intervals drive this feature will

help determine the dividing line between companions generated by core accretion versus gravitational/disk instability. The possibility of a drop-off in occurrence beyond 10 AU persists as well, though the large uncertainties at these wide separations prevent a firm conclusion.

The combination of RVs and absolute astrometry is a powerful tool for the detection and characterization of exoplanets. By breaking the RV mass-inclination degeneracy, this technique facilitates direct comparison of

dynamical and model masses across different detection methods and semi-major axis ranges. The upcoming release of Gaia DR4, expected December 2026,³ will both increase the available pool of giant companion-hosting stars and allow for even more precise orbital modeling, sharpening our understanding of the trends described in this work.

Software: `astropy` (Astropy Collaboration et al. 2018), `Orvara` (Brandt et al. 2021b), `numpy` (Harris et al. 2020), `scipy` (Virtanen et al. 2020),

REFERENCES

1997, ESA Special Publication, Vol. 1200, The HIPPARCOS and TYCHO catalogues. Astrometric and photometric star catalogues derived from the ESA HIPPARCOS Space Astrometry Mission

Akaike, H. 1974, A new look at the statistical model identification, *IEEE Transactions on Automatic Control*, 19, 716, doi: [10.1109/TAC.1974.1100705](https://doi.org/10.1109/TAC.1974.1100705)

Astropy Collaboration, Price-Whelan, A. M., Sipőcz, B. M., et al. 2018, The Astropy Project: Building an Open-science Project and Status of the v2.0 Core Package, *AJ*, 156, 123, doi: [10.3847/1538-3881/aabc4f](https://doi.org/10.3847/1538-3881/aabc4f)

Baraffe, I., Chabrier, G., Barman, T. S., Allard, F., & Hauschildt, P. H. 2003, Evolutionary models for cool brown dwarfs and extrasolar giant planets. The case of HD 209458, *A&A*, 402, 701, doi: [10.1051/0004-6361:20030252](https://doi.org/10.1051/0004-6361:20030252)

Bonnefoy, M., Marleau, G. D., Galicher, R., et al. 2014, Physical and orbital properties of β Pictoris b, *A&A*, 567, L9, doi: [10.1051/0004-6361/201424041](https://doi.org/10.1051/0004-6361/201424041)

Bowler, B. P., Blunt, S. C., & Nielsen, E. L. 2020, Population-level Eccentricity Distributions of Imaged Exoplanets and Brown Dwarf Companions: Dynamical Evidence for Distinct Formation Channels, *AJ*, 159, 63, doi: [10.3847/1538-3881/ab5b11](https://doi.org/10.3847/1538-3881/ab5b11)

Bowler, B. P., & Nielsen, E. L. 2018, in *Handbook of Exoplanets*, ed. H. J. Deeg & J. A. Belmonte, 155, doi: [10.1007/978-3-319-55333-7_155](https://doi.org/10.1007/978-3-319-55333-7_155)

Brandt, G. M., Michalik, D., Brandt, T. D., et al. 2021a, htof: A New Open-source Tool for Analyzing Hipparcos, Gaia, and Future Astrometric Missions, *AJ*, 162, 230, doi: [10.3847/1538-3881/ac12d0](https://doi.org/10.3847/1538-3881/ac12d0)

Brandt, T. D. 2021, The Hipparcos-Gaia Catalog of Accelerations: Gaia EDR3 Edition, *ApJS*, 254, 42, doi: [10.3847/1538-4365/abf93c](https://doi.org/10.3847/1538-4365/abf93c)

Brandt, T. D., Dupuy, T. J., Li, Y., et al. 2021b, orvara: An Efficient Code to Fit Orbits Using Radial Velocity, Absolute, and/or Relative Astrometry, *AJ*, 162, 186, doi: [10.3847/1538-3881/ac042e](https://doi.org/10.3847/1538-3881/ac042e)

Burrows, A., Hubbard, W. B., Lunine, J. I., & Liebert, J. 2001, The theory of brown dwarfs and extrasolar giant planets, *Reviews of Modern Physics*, 73, 719, doi: [10.1103/RevModPhys.73.719](https://doi.org/10.1103/RevModPhys.73.719)

Currie, T., Brandt, G. M., Brandt, T. D., et al. 2023, Direct imaging and astrometric detection of a gas giant planet orbiting an accelerating star, *Science*, 380, 198, doi: [10.1126/science.abo6192](https://doi.org/10.1126/science.abo6192)

De Rosa, R. J., Nielsen, E. L., Wahhaj, Z., et al. 2023, Direct imaging discovery of a super-Jovian around the young Sun-like star AF Leporis, *A&A*, 672, A94, doi: [10.1051/0004-6361/202345877](https://doi.org/10.1051/0004-6361/202345877)

Do Ó, C. R., O’Neil, K. K., Konopacký, Q. M., et al. 2023, The Orbital Eccentricities of Directly Imaged Companions Using Observable-based Priors: Implications for Population-level Distributions, *AJ*, 166, 48, doi: [10.3847/1538-3881/acdc9a](https://doi.org/10.3847/1538-3881/acdc9a)

Drażkowska, J., & Alibert, Y. 2017, Planetesimal formation starts at the snow line, *A&A*, 608, A92, doi: [10.1051/0004-6361/201731491](https://doi.org/10.1051/0004-6361/201731491)

Foreman-Mackey, D., Hogg, D. W., & Morton, T. D. 2014, Exoplanet Population Inference and the Abundance of Earth Analogs from Noisy, Incomplete Catalogs, *ApJ*, 795, 64, doi: [10.1088/0004-637X/795/1/64](https://doi.org/10.1088/0004-637X/795/1/64)

Franson, K., Bowler, B. P., Zhou, Y., et al. 2023, Astrometric Accelerations as Dynamical Beacons: A Giant Planet Imaged inside the Debris Disk of the Young Star AF Lep, *ApJL*, 950, L19, doi: [10.3847/2041-8213/acd6f6](https://doi.org/10.3847/2041-8213/acd6f6)

Fulton, B. J., Rosenthal, L. J., Hirsch, L. A., et al. 2021, California Legacy Survey. II. Occurrence of Giant Planets beyond the Ice Line, *ApJS*, 255, 14, doi: [10.3847/1538-4365/abfcc1](https://doi.org/10.3847/1538-4365/abfcc1)

³ <https://www.cosmos.esa.int/web/gaia/release>

Grether, D., & Lineweaver, C. H. 2006, How Dry is the Brown Dwarf Desert? Quantifying the Relative Number of Planets, Brown Dwarfs, and Stellar Companions around Nearby Sun-like Stars, *ApJ*, 640, 1051, doi: [10.1086/500161](https://doi.org/10.1086/500161)

Harris, C. R., Millman, K. J., van der Walt, S. J., et al. 2020, Array programming with NumPy, *Nature*, 585, 357–362, doi: [10.1038/s41586-020-2649-2](https://doi.org/10.1038/s41586-020-2649-2)

Hyodo, R., Ida, S., & Charnoz, S. 2019, Formation of rocky and icy planetesimals inside and outside the snow line: effects of diffusion, sublimation, and back-reaction, *A&A*, 629, A90, doi: [10.1051/0004-6361/201935935](https://doi.org/10.1051/0004-6361/201935935)

Ida, S., & Lin, D. N. C. 2004, Toward a Deterministic Model of Planetary Formation. II. The Formation and Retention of Gas Giant Planets around Stars with a Range of Metallicities, *ApJ*, 616, 567, doi: [10.1086/424830](https://doi.org/10.1086/424830)

Kratter, K., & Lodato, G. 2016, Gravitational Instabilities in Circumstellar Disks, *ARA&A*, 54, 271, doi: [10.1146/annurev-astro-081915-023307](https://doi.org/10.1146/annurev-astro-081915-023307)

Lagrange, A. M., Wilkinson, C., Málin, M., et al. 2025, Evidence for a sub-Jovian planet in the young TWA 7 disk, *Nature*, 642, 905, doi: [10.1038/s41586-025-09150-4](https://doi.org/10.1038/s41586-025-09150-4)

Lindegren, L., Klioner, S. A., Hernández, J., et al. 2021, Gaia Early Data Release 3. The astrometric solution, *A&A*, 649, A2, doi: [10.1051/0004-6361/202039709](https://doi.org/10.1051/0004-6361/202039709)

Macintosh, B., Graham, J. R., Ingraham, P., et al. 2014, First light of the Gemini Planet Imager, *Proceedings of the National Academy of Science*, 111, 12661, doi: [10.1073/pnas.1304215111](https://doi.org/10.1073/pnas.1304215111)

Macintosh, B., Graham, J. R., Barman, T., et al. 2015, Discovery and spectroscopy of the young jovian planet 51 Eri b with the Gemini Planet Imager, *Science*, 350, 64, doi: [10.1126/science.aac5891](https://doi.org/10.1126/science.aac5891)

McKee, C. F., & Ostriker, E. C. 2007, Theory of Star Formation, *ARA&A*, 45, 565, doi: [10.1146/annurev.astro.45.051806.110602](https://doi.org/10.1146/annurev.astro.45.051806.110602)

Moe, M., & Di Stefano, R. 2017, Mind Your Ps and Qs: The Interrelation between Period (P) and Mass-ratio (Q) Distributions of Binary Stars, *ApJS*, 230, 15, doi: [10.3847/1538-4365/aa6fb6](https://doi.org/10.3847/1538-4365/aa6fb6)

Nielsen, E. L., De Rosa, R. J., Macintosh, B., et al. 2019, The Gemini Planet Imager Exoplanet Survey: Giant Planet and Brown Dwarf Demographics from 10 to 100 au, *AJ*, 158, 13, doi: [10.3847/1538-3881/ab16e9](https://doi.org/10.3847/1538-3881/ab16e9)

Petigura, E. A., Marcy, G. W., Winn, J. N., et al. 2018, The California-Kepler Survey. IV. Metal-rich Stars Host a Greater Diversity of Planets, *AJ*, 155, 89, doi: [10.3847/1538-3881/aaa54c](https://doi.org/10.3847/1538-3881/aaa54c)

Pollack, J. B., Hubickyj, O., Bodenheimer, P., et al. 1996, Formation of the Giant Planets by Concurrent Accretion of Solids and Gas, *Icarus*, 124, 62, doi: [10.1006/icar.1996.0190](https://doi.org/10.1006/icar.1996.0190)

Raghavan, D., McAlister, H. A., Henry, T. J., et al. 2010, A Survey of Stellar Families: Multiplicity of Solar-type Stars, *ApJS*, 190, 1, doi: [10.1088/0067-0049/190/1/1](https://doi.org/10.1088/0067-0049/190/1/1)

Reggiani, M., & Meyer, M. R. 2013, Universality of the companion mass-ratio distribution, *A&A*, 553, A124, doi: [10.1051/0004-6361/201321631](https://doi.org/10.1051/0004-6361/201321631)

Rivera, E. J., Laughlin, G., Butler, R. P., et al. 2010, The Lick-Carnegie Exoplanet Survey: a Uranus-Mass Fourth Planet for GJ 876 in an Extrasolar Laplace Configuration, *ApJ*, 719, 890, doi: [10.1088/0004-637X/719/1/890](https://doi.org/10.1088/0004-637X/719/1/890)

Rosenthal, L. J., Fulton, B. J., Hirsch, L. A., et al. 2021, The California Legacy Survey. I. A Catalog of 178 Planets from Precision Radial Velocity Monitoring of 719 Nearby Stars over Three Decades, *ApJS*, 255, 8, doi: [10.3847/1538-4365/abe23c](https://doi.org/10.3847/1538-4365/abe23c)

Rosenthal, L. J., Knutson, H. A., Chachan, Y., et al. 2022, The California Legacy Survey. III. On the Shoulders of (Some) Giants: The Relationship between Inner Small Planets and Outer Massive Planets, *ApJS*, 262, 1, doi: [10.3847/1538-4365/ac7230](https://doi.org/10.3847/1538-4365/ac7230)

Schlafman, K. C. 2018, Evidence of an Upper Bound on the Masses of Planets and Its Implications for Giant Planet Formation, *ApJ*, 853, 37, doi: [10.3847/1538-4357/aa961c](https://doi.org/10.3847/1538-4357/aa961c)

Schwarz, G. 1978, Estimating the Dimension of a Model, *The Annals of Statistics*, 6, 461, doi: [10.1214/aos/1176344136](https://doi.org/10.1214/aos/1176344136)

Shu, F. H., Adams, F. C., & Lizano, S. 1987, Star formation in molecular clouds: observation and theory., *ARA&A*, 25, 23, doi: [10.1146/annurev.aa.25.090187.000323](https://doi.org/10.1146/annurev.aa.25.090187.000323)

Spiegel, D. S., Burrows, A., & Milsom, J. A. 2011, The Deuterium-burning Mass Limit for Brown Dwarfs and Giant Planets, *ApJ*, 727, 57, doi: [10.1088/0004-637X/727/1/57](https://doi.org/10.1088/0004-637X/727/1/57)

Van Zandt, J., & Petigura, E. A. 2024a, No Evidence for a Metallicity-dependent Enhancement of Distant Giant Companions to Close-in Small Planets in the California Legacy Survey, *AJ*, 168, 268, doi: [10.3847/1538-3881/ad8c3b10.1134/S1063772908070056](https://doi.org/10.3847/1538-3881/ad8c3b10.1134/S1063772908070056)

Van Zandt, J., & Petigura, E. A. 2024b, ethraid: A Simple Method for Characterizing Long-period Companions Using Doppler, Astrometric, and Imaging Constraints, *AJ*, 167, 250, doi: [10.3847/1538-3881/ad390b](https://doi.org/10.3847/1538-3881/ad390b)

Van Zandt, J., Petigura, E. A., Lubin, J., et al. 2025, The TESS–Keck Survey. XXIV. Outer Giants May Be More Prevalent in the Presence of Inner Small Planets, *AJ*, 169, 235, doi: [10.3847/1538-3881/adbbed](https://doi.org/10.3847/1538-3881/adbbed)

Venner, A., An, Q., Huang, C. X., et al. 2024, HD 28185 revisited: an outer planet, instead of a brown dwarf, on a Saturn-like orbit, *MNRAS*, 535, 90, doi: [10.1093/mnras/stae2336](https://doi.org/10.1093/mnras/stae2336)

Virtanen, P., Gommers, R., Oliphant, T. E., et al. 2020, SciPy 1.0: Fundamental Algorithms for Scientific Computing in Python, *Nature Methods*, 17, 261, doi: [10.1038/s41592-019-0686-2](https://doi.org/10.1038/s41592-019-0686-2)

Wilkinson, C., Charnay, B., Mazevert, S., et al. 2024, Breaking degeneracies in exoplanetary parameters through self-consistent atmosphere–interior modelling, *A&A*, 692, A113, doi: [10.1051/0004-6361/202348945](https://doi.org/10.1051/0004-6361/202348945)

Winn, J. N. 2022, Joint Constraints on Exoplanetary Orbits from Gaia DR3 and Doppler Data, *AJ*, 164, 196, doi: [10.3847/1538-3881/ac9126](https://doi.org/10.3847/1538-3881/ac9126)

Youdin, A. N., & Zhu, Z. 2025, Formation of Giant Planets, *arXiv e-prints*, arXiv:2501.13214, doi: [10.48550/arXiv.2501.13214](https://doi.org/10.48550/arXiv.2501.13214)

Zhang, J., Weiss, L. M., Huber, D., et al. 2025, Discovery of a Jupiter Analog Misaligned to the Inner Planetary System in HD 73344, *AJ*, 169, 200, doi: [10.3847/1538-3881/ada60a](https://doi.org/10.3847/1538-3881/ada60a)